The Role of the Middle Atmosphere in Simulations of the Troposphere during Northern Hemisphere Winter: Differences between High- and Low-Top Models

FABRIZIO SASSI

Space Science Division, Naval Research Laboratory, Washington, D.C.

R. R. GARCIA AND D. MARSH

National Center for Atmospheric Research, Boulder, Colorado*

K. W. HOPPEL

Remote Sensing Division, Naval Research Laboratory, Washington, D.C.

(Manuscript received 15 July 2009, in final form 12 April 2010)

ABSTRACT

This paper compares present-day simulations made with two state-of-the-art climate models: a conventional model specifically designed to represent the tropospheric climate, which has a poorly resolved middle atmosphere, and a configuration that is built on the same physics and numerical algorithms but represents realistically the middle atmosphere and lower thermosphere. The atmospheric behavior is found to be different between the two model configurations, and it is shown that the differences in the two simulations can be attributed to differences in the behavior of the zonal mean state of the stratosphere, where reflection of quasi-stationary resolved planetary waves from the lid of the low-top model is prominent; the more realistic physics in the high-top model is not relevant. It is also shown that downward propagation of zonal wind anomalies during weak stratospheric vortex events is substantially different in the two model configurations. These findings extend earlier results that a poorly resolved stratosphere can influence simulations throughout the troposphere.

1. Introduction

Coupled atmosphere–ocean climate models, and in particular most of those that have been used in the Intergovernmental Panel on Climate Change (IPCC) reports, typically have a poorly resolved middle atmosphere, and chemical composition is for the most part specified (Solomon et al. 2007). These models cannot represent ozone depletion or the complex couplings associated with changes of chemical composition and their effects on the dynamical and thermal structure of the middle atmosphere. Instead, such chemical–radiative–dynamical couplings have been studied with models that represent the middle atmosphere properly, resolving both its dynamics and the chemical/physical processes. The performance of these models is documented by international programs such as the Chemistry Climate Model Validation activity (CCMVal; Eyring et al. 2007) of the Stratospheric Processes and their Role in Climate (SPARC) study. Because of the cost associated with interactive chemistry and physics, models that have a good representation of the middle atmosphere are often run with prescribed sea surface temperatures (SSTs) and sea ice distributions (Eyring et al. 2005). The specification of the lower boundary condition (in this case the sea surface temperature) strongly constraints the tropospheric climate to the imposed state, limiting the ability to assess any effect of the middle atmosphere on the surface properties (Rind et al. 2005; Yukimoto and Kodera 2007).

While the dynamical variability in the middle atmosphere is by and large the result of upward-propagating

* The National Center for Atmospheric Research is sponsored by the National Science Foundation.

Corresponding author address: Dr. Fabrizio Sassi, Naval Research Laboratory, Space Science Division, 4555 Overlook Ave., SW, Washington, DC 20375.
E-mail: fabrizio.sassi@nrl.navy.mil

DOI: 10.1175/2010JAS3255.1

Report Documentation Page

Form Approved
OMB No. 0704-0188

1. REPORT DATE	2. REPORT TYPE	3. DATES COVERED
APR 2010		**00-00-2010 to 00-00-2010**

4. TITLE AND SUBTITLE	5a. CONTRACT NUMBER
The Role of the Middle Atmosphere in Simulations of the Troposphere during Northern Hemisphere Winter: Differences between High- and Low-Top Models	5b. GRANT NUMBER
	5c. PROGRAM ELEMENT NUMBER
6. AUTHOR(S)	5d. PROJECT NUMBER
	5e. TASK NUMBER
	5f. WORK UNIT NUMBER
7. PERFORMING ORGANIZATION NAME(S) AND ADDRESS(ES) **Naval Research Laboratory,Space Science Division,Washington,DC,20375**	8. PERFORMING ORGANIZATION REPORT NUMBER
9. SPONSORING/MONITORING AGENCY NAME(S) AND ADDRESS(ES)	10. SPONSOR/MONITOR'S ACRONYM(S)
	11. SPONSOR/MONITOR'S REPORT NUMBER(S)

12. DISTRIBUTION/AVAILABILITY STATEMENT
Approved for public release; distribution unlimited

13. SUPPLEMENTARY NOTES

14. ABSTRACT

This paper compares present-day simulations made with two state-of-the-art climate models: a conventional model specifically designed to represent the tropospheric climate, which has a poorly resolved middle atmosphere, and a configuration that is built on the same physics and numerical algorithms but represents realistically the middle atmosphere and lower thermosphere. The atmospheric behavior is found to be different between the two model configurations, and it is shown that the differences in the two simulations can be attributed to differences in the behavior of the zonal mean state of the stratosphere, where reflection of quasistationary resolved planetary waves from the lid of the low-top model is prominent; the more realistic physics in the high-top model is not relevant. It is also shown that downward propagation of zonal wind anomalies during weak stratospheric vortex events is substantially different in the two model configurations. These findings extend earlier results that a poorly resolved stratosphere can influence simulations throughout the troposphere.

15. SUBJECT TERMS

16. SECURITY CLASSIFICATION OF:			17. LIMITATION OF ABSTRACT	18. NUMBER OF PAGES	19a. NAME OF RESPONSIBLE PERSON
a. REPORT	b. ABSTRACT	c. THIS PAGE			
unclassified	**unclassified**	**unclassified**	**Same as Report (SAR)**	**17**	

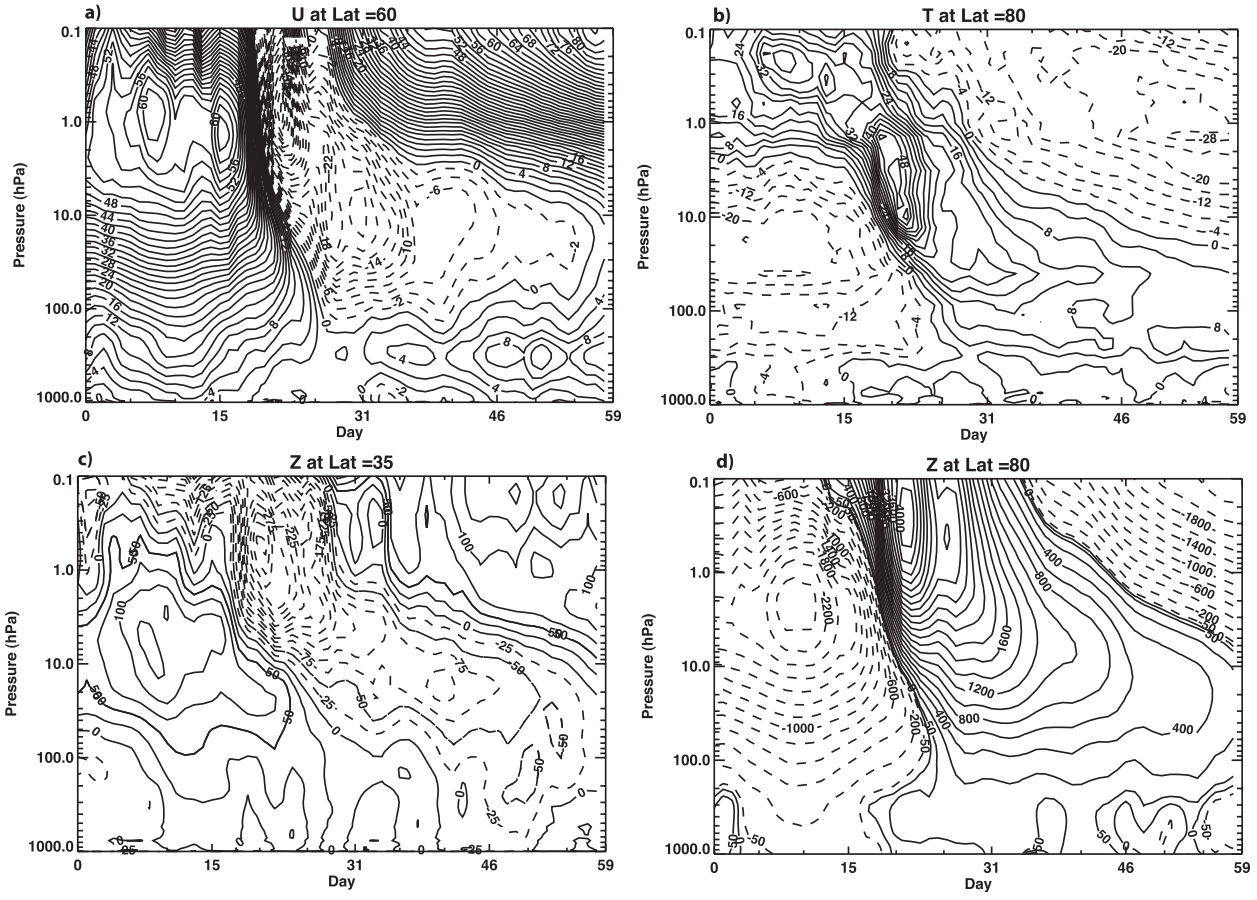

FIG. 1. NOGAPS-ALPHA data assimilation system for January and February 2009. (a) Zonal mean zonal wind at 60°N. Contour interval (CI) is 2 m s^{-1}. (b) Anomaly of the zonal mean temperature at 80°N. CI is 4 K. (c) Anomaly of the zonal mean geopotential height at 35°N. CI is 25 m. (d) Anomaly of the zonal mean geopotential height at 80°N. CI is 200 m; additional ±50-m contours are plotted for emphasis. Anomalies are calculated with respect to the time mean for January and February. The abscissa shows the days from 1 Jan (day = 0) to 28 Feb (day = 59).

disturbances from the troposphere (Charney and Drazin 1961; Sassi et al. 2004; Polvani and Waugh 2004; Manzini et al. 2006; Liu et al. 2009), the fact that the middle atmosphere may affect some properties of the tropospheric simulation has been the subject of studies since the seminal papers of Boville (1984) and Boville and Cheng (1988). In the first of these studies, the stratospheric simulation is artificially degraded, resulting in noticeable changes of mean climate properties of the tropospheric simulation. In the second, the lid is raised to allow a better resolution of the stratospheric circulation; the resulting changes in the tropospheric simulation are remarkably similar to the earlier paper.

Some of aforementioned studies focus on the Northern Hemisphere winter and the sudden stratospheric warmings (SSWs) that occur, on average, about once every two years in the stratosphere (Charlton et al. 2007). The SSWs are large perturbations that may displace the polar vortex off its circumpolar symmetry (minor warmings) or even reverse the stratospheric circulation altogether (major warmings), producing an easterly zonal flow where normally the winds are westerly. Several studies have indicated that major SSWs can influence a deep layer of the atmosphere through downward-propagating zonal anomalies (Kodera et al. 2000; Baldwin and Dunkerton 2001) or wave reflection (Perlwitz and Harnik 2004).

When SSW events are large, the impact in the lower atmosphere is most evident. An example is given in Fig. 1, which shows the zonal mean zonal wind at 60°N (Fig. 1a), the anomaly of zonal mean temperature at 80°N (Fig. 1b), and the anomalies of geopotential height at 35°N and 80°N during January and February 2009 produced by the data assimilation system of the Navy Operational Global Atmospheric Predictions System–Advanced Level Physics and High Altitude (NOGAPS-ALPHA) (Figs. 1c,d; Hoppel et al. 2008; Eckermann et al. 2009). All anomalies are calculated with respect to the climatological time mean for the two-month period January–February. This

period includes the sudden stratospheric warming of 2009, which is also documented in Manney et al. (2009). The zonal mean wind (Fig. 1a) undergoes a very rapid reversal around 24 January 2009: the reversal begins in the lower mesosphere around the middle of January but descends rapidly to the 10-hPa level in less than 5 days, and to 100 hPa in about 10 days. As pointed out by Manney et al. (2009), the magnitude and persistence of this event makes it a ''record-breaking stratospheric warming.'' In fact, the zonal mean circulation remains easterly throughout the remainder of the winter in the lower stratosphere with some indication of changes occurring also in the troposphere. The polar temperature anomaly (Fig. 1b) shows a large positive anomaly accompanying the evolution of the zonal mean zonal wind: the largest temperature anomaly exceeds 50 K at 10 hPa. The anomaly weakens following the peak of the event, but it persists throughout the assimilation period. The geopotential height anomaly over the Arctic (Fig. 1d) shows the expected positive anomaly, which peaks in the lower mesosphere near 20 January and descends below 100 hPa by the end of January. This anomaly contrasts with the climatological behavior, wherein the anomaly with respect to the January–February time average is negative. Similar to the case of the zonal mean wind (Fig. 1a), but much more evident now, the height anomaly shows a dramatic change throughout the column (from the troposphere throughout the stratosphere) between a negative height anomaly before the stratospheric event to a positive height anomaly after the stratospheric event. In the subtropics (Fig. 1c), the morphology of the height anomaly mirrors that of the high-latitude anomaly but with opposite sign, illustrating the expected seesaw pattern during stratospheric events: the height increases over the Arctic and decreases at lower latitudes. This seesaw pattern has been argued to affect the troposphere in the Northern Hemisphere (Baldwin and Dunkerton 1999). It is interesting to note that around day 40 and later (i.e., after 9 February 2009) the subtropical lower atmosphere is invaded by the negative height anomaly descending from the stratosphere. It should be borne in mind that the persistence and magnitude of the anomalies described in Fig. 1 are not those of a typical SSW; this event is truly a record-breaking warming.

While Boville and Cheng (1988) discuss the time-mean response to the model configuration in the middle atmosphere, the evidence from Fig. 1 poses an interesting question regarding the representation of variability in the middle atmosphere. Boville and Cheng showed that although the lid reflects planetary waves and directly influences the wave structure in the stratosphere and the zonal circulation thereof, the lid has little *direct* influence on the tropospheric waves. Even so, the behavior of the stationary planetary waves is different in the model configurations with low and high upper boundaries, and Boville and Cheng argue that those changes follow from modest differences of the zonal circulation of the lower stratosphere. Recognizing that causality between changes in planetary waves and changes in the zonal mean state in a GCM remains ambiguous, we take a step beyond Boville and Cheng's findings and describe the atmospheric variability during different stratospheric states in models with a well (and poorly) resolved middle atmosphere. The question, therefore, that still remains unanswered and is at the core of this study is how important is the representation of the middle atmosphere in this context.

To answer this question, we run a simulation that uses a climate–chemistry model with a lid at 140 km, with composition and chemical boundary conditions typical of the present-day atmosphere. We compare the results of this model to a similar simulation carried out with a climate model specifically designed to represent the lower atmosphere and with a lid at 40 km. This model does not have interactive chemistry and has a poor vertical resolution in the middle atmosphere. In both cases our model experiments are coupled to a mixed layer ocean to prevent specified sea surface temperatures from constraining the tropospheric response. A description of the models and run configurations, together with our analysis methodology, is provided in section 2. In section 3, we discuss the mean climate behavior during December–February (DJF). We examine the response of the two simulations during northern winter (DJF). Section 4 deals with the life cycle of weak stratospheric events (i.e., episodes during which the polar night jet becomes significantly weaker than normal). Conclusions are presented in section 5.

2. Models, simulations, and analysis

a. Models

The Community Atmosphere Model, version 3 (CAM3) is the standard atmospheric component of the National Center for Atmospheric Research (NCAR) Community Climate System Model, version 3 (CCSM3). The quality of the climate simulated with CAM3 is described in Collins et al. (2006). The model lid in CAM3 is at 3.5 hPa with 26 levels. There are 18 levels in the troposphere (pressure $>$ 100 hPa) with a vertical resolution ranging from less than 100 m near the surface to 1 km in the upper troposphere; vertical resolution decreases rapidly in the stratosphere where there are only eight levels. The vertical resolution between the model lid and the first level below it is 5.2 km. The horizontal resolution used

in this study is 1.9° of latitude by 2.5° of longitude. The dynamical equations are solved using the Lin (2004) finite volume scheme, which is a flux mass-conserving algorithm. To conserve mass in the whole domain as well, mass is not allowed to escape from the upper boundary of the model: this is achieved by imposing a zero vertical velocity (more accurately, zero time derivative of pressure) at the model top interface. The model does not employ any form of Rayleigh friction or any explicit hyperviscosity to dissipate disturbances approaching the lid; however, a divergence damper that reduces the amplitude of divergent motions is implemented near the model lid. The divergence damper controls the amplitude of resolved gravity waves at high wavenumbers, and prevents spurious accumulation of energy at the high-wavenumber tail of the spectrum (P. Lauritzen 2009, personal communication). Because of the zero flux upper boundary condition, momentum conservation is satisfied for resolved wave motions. CAM3 also employs an orographic gravity wave parameterization (McFarlane 1987), which accounts for unresolved mesoscale waves excited by subgrid-scale orography. At this time, the gravity wave parameterization does not strictly conserve momentum, as discussed in Shaw and Shepherd (2007); however, because the model lid is at about 3 hPa, essentially all of the momentum carried by orographic gravity waves is deposited in the model domain below the upper boundary, so nonconservation issues can be neglected.

The Whole Atmosphere Community Climate Model, version 3 (WACCM3) is a climate–chemistry general circulation model developed at NCAR, based on the infrastructure of CAM3. In the lower atmosphere WACCM3 is identical to CAM3 and makes use of the same parameterizations and dynamical solution method. The vertical domain of WACCM3 extends to 5.9×10^{-6} hPa (~140 km geometric height) with 66 levels. The vertical resolution is identical to that of CAM3 up to 100 hPa but is substantially finer above the tropopause: in the lower stratosphere the vertical resolution ranges from 1.5 km near the tropopause to about 2 km near the stratopause, and in the mesosphere the vertical resolution is half of the local scale height and remains so up to the model lid. WACCM3 can be used in place of CAM3 as the atmospheric component of CCSM3.

Global tropospheric climate properties (like annual globally averaged surface temperature) are statistically indistinguishable between the two model runs (not shown). WACCM can be regarded as an extended version of the CAM into the middle and upper atmosphere with interactive chemistry and physics. To reproduce realistically the middle and upper atmosphere, several physical parameterizations are added to WACCM: a parameterization of unresolved, nonorographic gravity waves; treatment of the nonlocal thermodynamic equilibrium radiative relaxation, including cooling by nitric oxide in the thermosphere; molecular diffusion with species separation; and interactive chemistry and physics up to 140 km. A detailed description of WACCM3 can be found in Garcia et al. (2007), the model's dynamical climatology is discussed in Richter et al. (2008), and the chemical solution scheme is described in Kinnison et al. (2007).

b. Simulations

To increase the interactivity of the simulation and look at the surface response without the constraints of a specified boundary condition, both WACCM and CAM are coupled to a mixed layer or slab ocean model (SOM). The SOM employed in this study is an option in the configuration of CAM, and it is fully described in Collins et al. (2004). The SOM allows a simplified but still interactive treatment of the mixed layer ocean temperature, the thermodynamic sea ice, snow depth, and ice thickness and coverage. The energy transport (Q-flux) due to seasonally changing deep ocean water and horizontal transport in the mixed layer is estimated from an atmosphere stand-alone simulation that provides the surface heat budget and exchange with the atmosphere.

The simulation with WACCM uses fully interactive chemistry and physics, whereas CAM has uniform distributions of some greenhouse gases (CO_2, N_2O, CH_4, CFC11, and CFC12) and a climatological (monthly varying) distribution of ozone (see Sassi et al. 2005). WACCM3 and CAM3 are configured for 1995 chemical composition and solar minimum conditions. The atmospheric stand-alone models are run with prescribed climatological SST for 15 years. The monthly averaged output of the last 10 years is used to calculate the Q-fluxes. The Q-fluxes are used as input to the SOM. When the GCMs are configured to use the SOM, the SSTs become a prognostic variable. We carried out two simulations. The first simulation uses WACCM3 coupled to the SOM with chemical composition corresponding to 1995 and solar minimum irradiance (hereafter simply called WACCM). In this case, the value of carbon dioxide in the well-mixed atmosphere is 357 ppmv. The second simulation (hereafter simply called CAM) uses CAM3 coupled to the SOM, with the same values of greenhouse gases in the well-mixed atmosphere used in WACCM. It should be borne in mind that CAM does not have any chemistry and the abundances of these constituents are not subject to change. The WACCM simulation is 51 years long; the CAM simulation is 55 years long. Both simulations are started from the initial conditions produced at the end of the atmosphere stand-alone simulations used to produce the Q-fluxes.

c. Analysis data

Daily upper air data of zonal wind and temperature from the 40-yr European Centre for Medium Range Weather Forecast (ECMWF) Re-Analysis (ERA-40; http://dss.ucar.edu/pub/era40/) between 1958 and 2001 is used for comparison with the model simulations. Diurnally averaged sea level pressure (SLP) from ERA-40 is also used to compare with the surface response calculated by the models.

We also use daily data from the Naval Research Laboratory Atmospheric Variational Data Assimilation System (NAVDAS) product (Hoppel et al. 2008; Eckermann et al. 2009). This dataset is available only after 2004; we present results from recent SSWs in 2006, 2008, and 2009.

d. Identification of the extreme stratospheric events

A major stratospheric warming is defined by the World Meteorological Organization (WMO) as a reversal of the zonal mean zonal wind at 10 hPa and 60°N. As noted earlier, such events are not so common in observations, occurring approximately once every two years. In addition, major warmings that meet the WMO criteria are often less frequent in GCMs than in observations (e.g., Charlton et al. 2007), which limits the ability to obtain statistically significant results if the WMO criteria were used to select the disturbed-stratosphere events. Therefore, the identification of the stratospheric events used here follows Limpasuvan et al. (2004): a weak (strong) vortex event is identified when the difference between the time-mean zonally averaged zonal wind and the daily zonally averaged zonal wind at 60°N and 50 hPa exceeds +1.5 (−1.5) times the daily standard deviation. The choice of these thresholds is somewhat arbitrary and in our case was guided by the desire to reproduce results that are similar in magnitude to those obtained by Baldwin and Dunkerton (2001; cf. their Fig. 3 and our Fig. 7c). For each event so identified we define the midpoint (central time) of the event as the middle of the period during which the daily zonal wind standard deviation exceeds the threshold. The composite behavior for the stratospheric event is calculated by averaging all fields of interest during three time intervals referred to the midpoint of the event: a growth stage that includes days −22 to −8, a mature stage that includes days −7 to +7, and a declining stage that includes days +8 to +22. Except when noted otherwise, the anomalies are obtained by subtracting the mean seasonal cycle. The stratospheric events are identified in CAM and WACCM from daily output of the zonal mean wind. ERA-40 daily winds are used to identify the stratospheric events between 1958 and 2001. With this method we identify 15 weak stratospheric events (WSEs) and 46 strong stratospheric events (SSEs) in CAM, 18 WSEs and 53 SSEs in WACCM, and 43 WSEs and 41 SSEs in ERA-40.

3. Northern Hemisphere winter behavior

We focus on northern winter (DJF). This season is important because it has the largest forced dynamical variability, which is thought to exert an upward and downward influence (Kodera et al. 2000; Baldwin and Dunkerton 2001).

a. Zonal mean behavior

Figure 2 shows the DJF (top) zonal mean zonal wind and (bottom) zonal mean temperature from the WACCM (Figs. 2a,d) and CAM (Figs. 2b,e) simulations and from the analysis (Figs. 2c,f). Compared to the analysis, both model configurations reproduce correctly the location and strength of the tropospheric subtropical jet, but they tend to have too strong a zonal circulation near the surface; this problem is alleviated only with the inclusion of an additional surface drag (Richter et al. 2010). The zonal winds illustrate different behavior in the lower stratosphere: the observed state has a weak zonal circulation, with the 20 m s^{-1} isoline closing off near 20 km; WACCM winds are somewhat stronger than the real atmosphere, but overall in agreement; CAM, instead, shows a much stronger zonal wind (~30 m s^{-1}) at 20 km. In the middle stratosphere (30–40 km), CAM has much too strong a zonal circulation with winds exceeding 50 m s^{-1} near the lid of the model, about twice as large as the analysis or WACCM in the same location.

The zonal mean temperature structures (Figs. 2d–f) are quite close in the two model configurations and in the analysis up to about 20 km; above this altitude the polar vortex is much colder in the CAM configuration, showing a zonal mean temperature that is in excess of 10 K colder than in the observed state. On the other hand, WACCM shows a thermal structure that is more in line with the analysis, with the coldest air found between 20 and 30 km at the pole. Both models differ from the analysis in that they produce a cold pole bias that reaches below 10 km. This cold pole bias can be partly alleviated with the use of a new gravity wave parameterization (Richter et al. 2010). It is worth repeating that the zonal structure above 30 km in CAM is not realistic: the zonal wind is too strong and the temperature, which follows from geostrophic balance, is too cold.

Figure 3 compares the zonal mean zonal wind of the two model configurations and of the analysis during the mature stages of the (top) WSE and (bottom) SSE. The identification of the extreme stratospheric events is as described above (section 2d), except that in the calculation of the wind composites the time-mean behavior is

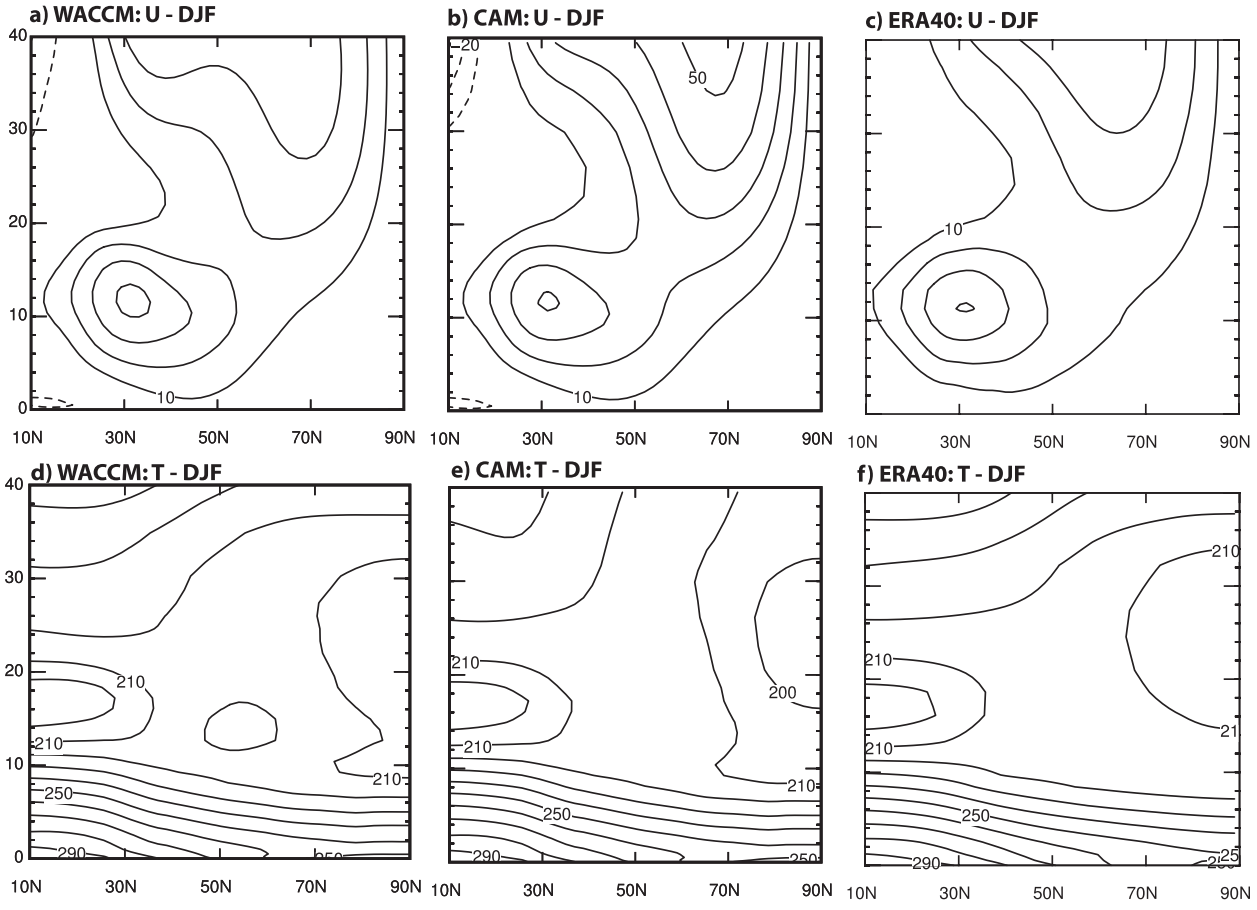

FIG. 2. DJF average of the (a)–(c) zonal mean zonal wind and (d)–(f) zonal mean temperature for the (a),(c) WACCM and (b),(e) CAM model configurations and (c),(f) ERA-40 analysis. Contour intervals are 10 m s^{-1} and 10 K for wind and temperature, respectively. No zero contours are plotted.

not subtracted. The ERA-40 analysis shows a substantial weakening of the stratospheric jet during a WSE (Fig. 3c) compared to its time-mean behavior (Fig. 2c). In both models (Figs. 3a,b) a similar weakening is obtained during WSEs in the stratosphere. Although substantially weakened compared to its time mean, CAM (Fig. 3b) maintains slightly stronger westerlies at 70°N and 20 km compared to both WACCM and ERA-40. This results in a more pronounced deflection of wave activity away from the polar vortex in CAM (as shown below in connection with Fig. 5). Note that the magnitude of the absolute change between the stratospheric events (Fig. 3) and their climatologies (Fig. 2) is disproportionately large in CAM compared to both WACCM and the analysis.

In the case of SSE (Figs. 3d–f) CAM is substantially stronger than the observed state with a strong jet of about 60 m s^{-1} at 40 km and 70°N. WACCM has a somewhat weaker jet than observed during the SSE, less than 40 m s^{-1} at 40 km. It is worth noting that the models' SSEs (Figs. 3d,e) are much closer to their respective climatologies (Figs. 2a,b) than the analysis (Fig. 3f) is to its climatology (Fig. 2c); while the real atmosphere has weak and strong events that are well differentiated from the observed mean state, the two models show a behavior during strong events that is closer to their mean state. This is a direct consequence of the paucity of WSEs in the models compared to the ERA-40 (cf. section 2d): as fewer SSWs occur in the models, all other things being equal, the time mean is dominated by the strong events.

b. Quasi-stationary planetary waves

The behavior shown in Figs. 2 and 3 illustrates that CAM and WACCM behave differently during Northern Hemisphere winter. Some aspects of the described climatology, like the more isolated and colder stratospheric vortex during winter in a model with a low top, were also documented by Boville and Cheng (1988). They argued that these features are caused by wave reflection, showing a nearly vertical alignment of the phase lines of geopotential height in the proximity of the lid of the model

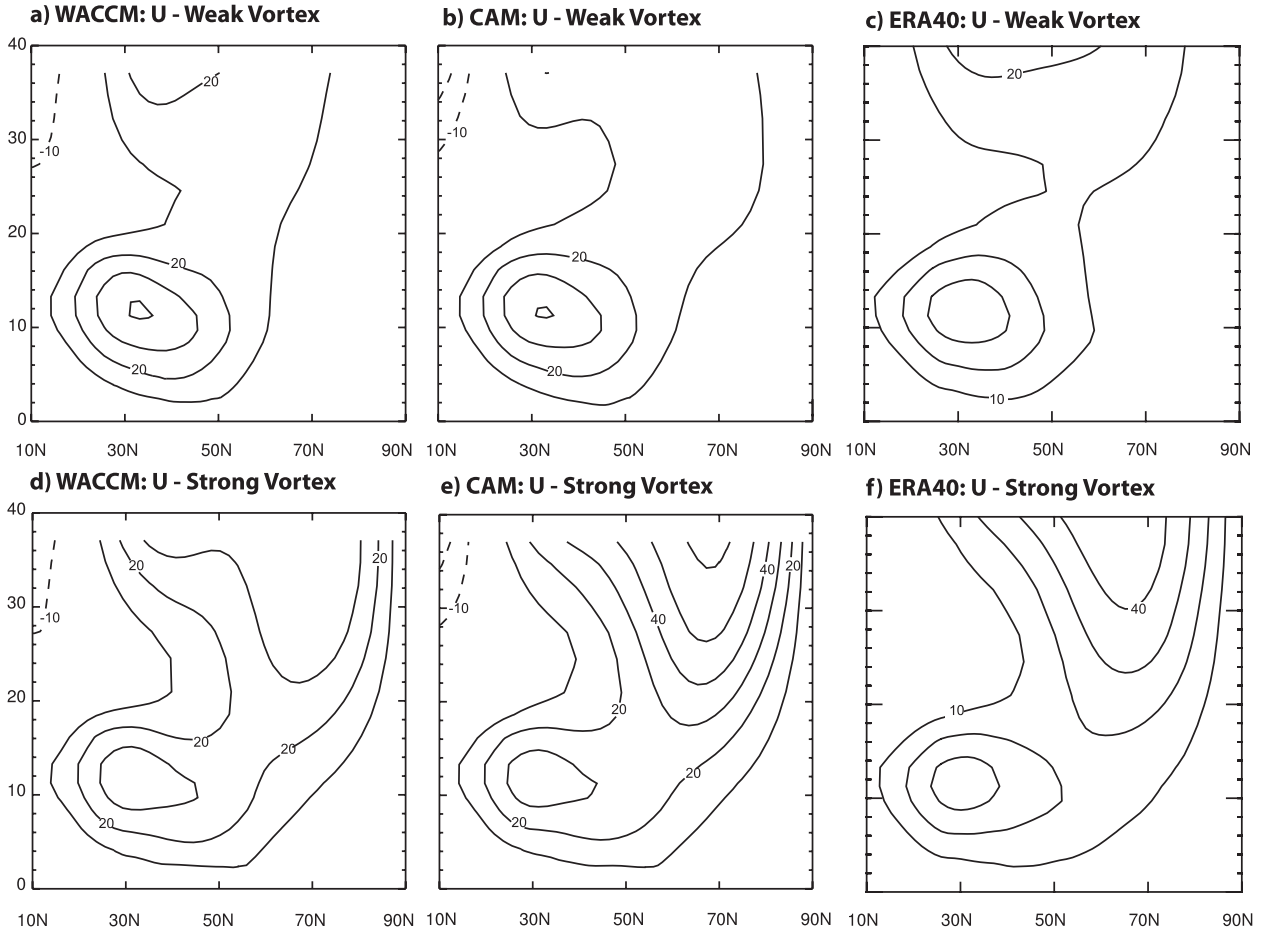

FIG. 3. Composite average of the zonal mean zonal wind during (top) WSEs and (bottom) SSEs for (a),(d) WACCM, (b),(e) CAM, and (c),(f) ERA-40. Contour interval is 10 m s^{-1}. See text for details.

with a low top. The progressively stronger vertical alignment of the phase lines in this model differs from the westward tilt with height associated with upward-propagating planetary waves and results ultimately in different eddy fluxes near the model top. In Fig. 4, we show the amplitude and the phase of stationary wave 1 of geopotential height averaged in DJF for WACCM (Figs. 4a,d), CAM (Figs. 4b,e), and ERA-40 (Figs. 4c,f). The amplitude in both models (Figs. 4a,b) is significantly smaller than in the reanalysis (Fig. 4c): around 20 km and 70°N, both WACCM and CAM wave-1 amplitudes are about 50 m, whereas in ERA-40 the amplitude is about 150 m; at 40 km and 70°N the WACCM wave-1 amplitude is 350 m, CAM is 300 m, and ERA-40 is 900 m. The smaller wave-1 amplitude in the model simulations is consistent with the few full reversals of the zonal mean circulation at 10 hPa and 60°N in both models. Notice that the amplitude of wave 1 in WACCM is somewhat larger than the amplitude in CAM: the models' wave-1 amplitudes around 40 km are within less than one standard deviation of each other (not shown), which indicates that in fact the CAM and WACCM wave-1 amplitudes are not statistically distinguishable. While this is in apparent contrast with the results of Boville and Cheng, the zonal wind structure in our model simulations (Fig. 2) by itself tends to produce different wave amplitudes. As we show next, the important aspect is the behavior of the planetary wave phase, which leads to different wave–zonal mean flow interaction.

In both model configurations, the wave-1 phase shows a westward tilt with height up to about 20 km, which is consistent with the expected upward-propagating nature of planetary waves as shown by the reanalysis (Fig. 4f). However, there are some marked differences between the two models in the stratosphere: the westward tilt is much reduced in the model with a low top (Fig. 4b), and in fact the phase lines become almost constant with height above 20 km and poleward of 50°N (see the partially highlighted contours). The behavior in CAM is in contrast with the phase structure in ERA-40,

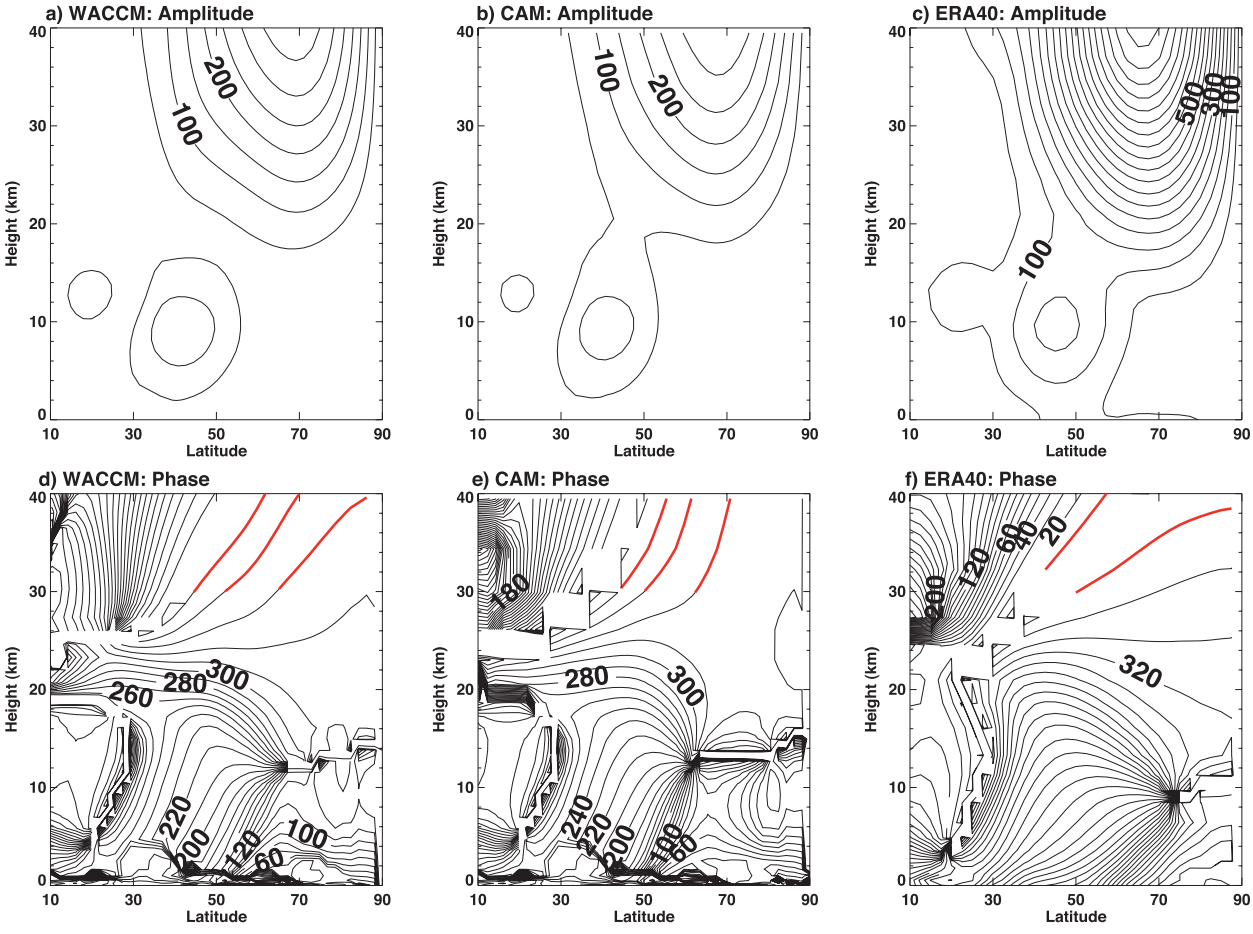

FIG. 4. DJF stationary wave-1 (top) amplitude and (bottom) phase of geopotential height from (a),(d) the WACCM simulation, (b),(e) CAM, and (c),(f) ERA-40. Contour interval for the amplitude is 50 m; phase lines are plotted every 10°. Phase lines above 30 km and poleward of 50°N are highlighted in red for emphasis.

which shows a continuous and gentle phase tilt with height.

The different phase structure in the two models reflects differences in wave propagation and implies differences in dissipation. This effect can be illustrated by the meridional momentum flux and the Eliassen–Palm (EP) flux divergence (EPD), which describe the zonal mean momentum transport by all resolved waves; at middle and high latitudes, where the geostrophic approximation is dominant, they closely describe the momentum transport associated with Rossby waves. Averaged during DJF and over the duration of the simulation, they then illustrate the behavior of Rossby waves. The resulting fields are shown in Fig. 5. The meridional momentum flux (Fig. 5a) in WACCM (red contours) shows the expected maximum at midlatitudes, increasing with height. The difference CAM minus WACCM (black contours) indicates an amplification of the momentum flux near the model lid of CAM, which is a result of trapping of upward-propagating wave activity by the lid of the low-top model. On the other hand, the vertical component of the Eliassen–Palm flux (not shown) is reduced in the low-top model, consistent with trapping of wave activity by the model lid. The EPD in WACCM (Fig. 5b; red contours) has the expected structure, which produces an easterly acceleration throughout the stratosphere, and is consistent with our understanding of the role played by planetary waves, which carry easterly momentum from the tropospheric sources near the surface to the middle atmosphere where they are dissipated. On the other hand, the difference CAM minus WACCM (Fig. 5b; black contours) shows a large westerly (positive) source of momentum almost everywhere above 20 km in the winter hemisphere. In fact, the EPD in CAM (not shown) is by and large positive in the winter stratosphere above 30 km, poleward of 50°N. Both the amplification of the momentum flux (Fig. 5a) and the westerly source of momentum (Fig. 5b) coincide with the region of wave

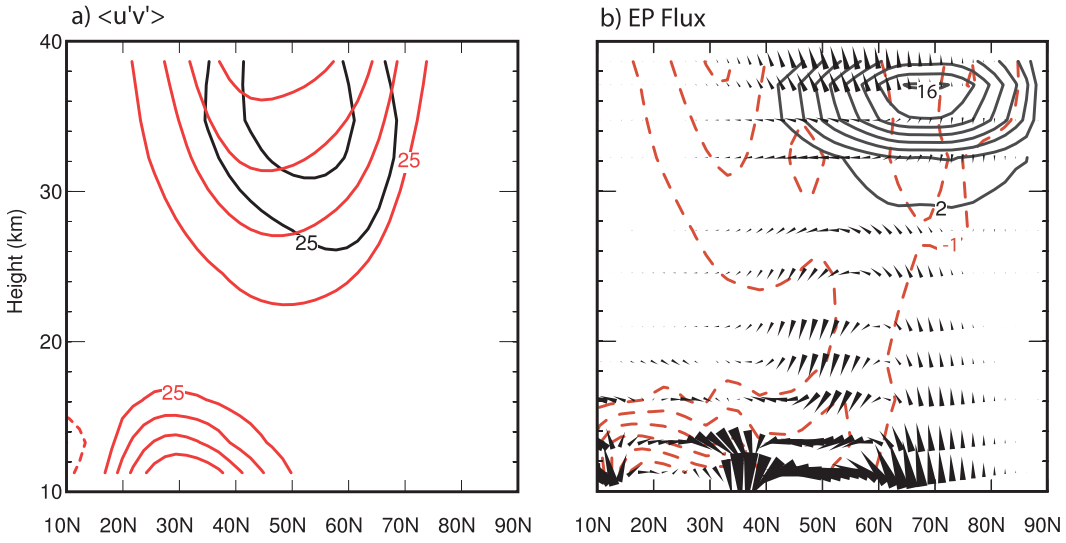

FIG. 5. (a) Meridional momentum flux ($m^2\ s^{-2}$) and (b) EP flux divergence ($m\ s^{-1}\ day^{-1}$) averaged during DJF from the WACCM simulation (red) and the difference CAM minus WACCM (black). Contour interval is 25 $m^2\ s^{-2}$ in (a) for both black and red contours. In (b) the contour interval is 1 $m\ s^{-1}\ day^{-1}$ for the red contours and 2 $m\ s^{-1}\ day^{-1}$ for the black contours. No zero contours are plotted. The arrows in (b) show the direction of the difference between the vector ($\mathbf{F}_y$, $\mathbf{F}_z$) of CAM minus WACCM, where $\mathbf{F}_{y,z}$ are the horizontal and vertical components of the EP flux.

reflection (Fig. 4). The difference between the components of the Eliassen–Palm fluxes of CAM and WACCM (arrows in Fig. 5b) reinforces the above argument by illustrating the source of momentum above 30 km. The EP flux difference in the lower stratosphere and upper troposphere shows that the CAM fluxes have an equatorward and downward bias compared to WACCM. Below 30 km, the flux anomalies in Fig. 5 illustrate a deflection of the Rossby waves away from the polar vortex with resulting changes of the wave propagation both in the stratosphere and in the troposphere.

Figure 6 shows the difference between CAM and WACCM of the zonal mean wind averaged during DJF. The difference in NH zonal mean zonal wind between the two model simulations corresponds closely to the EPD difference shown in Fig. 5b. As expected, the largest changes are near the lid of CAM and show a strengthening of the polar night jet, but the zonal mean wind difference now extends into the troposphere. It is worth noting that even though the wind difference is not large, statistical significance extends to near the ground at the midlatitudes of the winter hemisphere.

c. *Surface behavior*

Changes in SLP have been related to different conditions in the middle atmosphere (Boville 1984; Baldwin and Dunkerton 2001). This happens, for example, when the stratospheric vortex is weakened or reversed as during a sudden stratospheric warming; then, the mean meridional circulation is strengthened and more mass is transported into the polar cap. The reverse occurs during periods of strengthening of the polar vortex, when the mass over the polar cap decreases. Figure 7 illustrates the SLP anomaly associated with WSEs between November and March in the two model configurations and in the reanalysis. During WSEs the reanalysis (Fig. 7c) shows an increase of SLP over the Arctic with a peak (5 hPa) over northern Siberia. The high-latitude increase is accompanied by a smaller decrease (~ -2 hPa) at midlatitudes over southern Europe. This seesaw pattern is a well-known aspect of the atmospheric dynamics and has been documented by other authors (see Baldwin and Dunkerton 2001). The Arctic structure is partly zonally symmetric, with a positive anomaly extending over the North American continent. There are two main regions of negative response centered over southern Europe and the northern Pacific Ocean.

The simulations show several similarities in the high-latitude response of SLP. Common to both model simulations is an excessive Arctic anomaly during WSE compared to ERA-40 data. The CAM simulation (Fig. 7b) shows a much stronger northern European anomaly (-13 hPa) compared to the reanalysis. The WACCM simulation (Fig. 7a) has a somewhat weaker anomaly (~ 9 hPa) than CAM, but both model anomalies are substantially larger than the reanalysis anomaly (Fig. 7c). The high-latitude anomaly in CAM is much more confined to the Arctic than in WACCM, resulting in

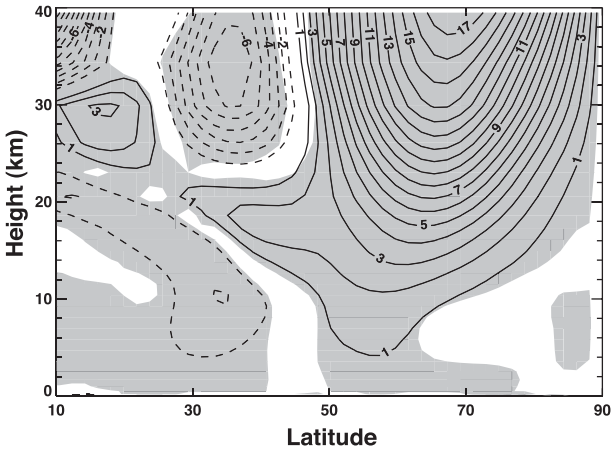

FIG. 6. DJF zonal mean zonal wind difference CAM minus WACCM, plotted only for the NH. Contour interval is 1 m s^{-1} and no zero contours are plotted. The shaded areas are significant at least at the 95% level based on a *t* test with 50 degrees of freedom.

a notable absence of the positive anomaly over North America seen in the real atmosphere. The observed positive SLP anomaly produces anomalous surface winds that are southerly and easterly over North America. On the other hand, the more poleward confinement of the Arctic anomaly in CAM leads to anomalous surface winds during WSEs that follow a westerly zonal course. WACCM is somewhat more in line with the reanalysis, although the pattern of anomalies is distorted by the amplified polar magnitudes. Another notable difference between the two simulations is in the behavior of the Aleutian low: CAM shows a substantial increase (2 hPa) of SLP during a WSE over the eastern edge of the Aleutian Islands, whereas WACCM indicates a decrease (−3 hPa) of pressure in the same location, more similar to the modest deepening seen in the reanalysis (−1 hPa).

Particularly during northern winter, these differences in SLP reflect a different behavior of the atmosphere above the surface. Because the differences are most marked during WSEs, we examine in detail the atmospheric behavior during these events in the next section.

4. Life cycle of weak stratospheric events

In section 3 we have shown that during NH winter differences of the zonal mean behavior between the two model configurations extend into the troposphere (Fig. 6). It is important to remember that the different character of the polar night jet in the two simulations results directly from wave reflection at the model lid in CAM (Fig. 5). In this section we examine in greater detail how this behavior is connected with the evolution of the stratospheric events that were described in section 3.

We examine the composite behavior of the stratospheric events during selected time intervals that describe the growth, mature and decline stages of those events (see section 2d for the definition of these stages). Figures 8–10 show the composite anomalies of the zonal mean zonal wind during WSE in WACCM (Fig. 8), CAM (Fig. 9), and the ERA-40 analysis (Fig. 10). The composite anomaly in WACCM compares well with the observed behavior. During the growth phase (Fig. 8a), an easterly wind anomaly begins to invade the stratosphere from higher levels. At the mature stage (Fig. 8b), the easterly wind anomaly reaches its largest magnitude between 30 and 40 km and is accompanied by a warming of the polar cap of several degrees (not shown); moreover, the geopotential surfaces (not shown) are elevated

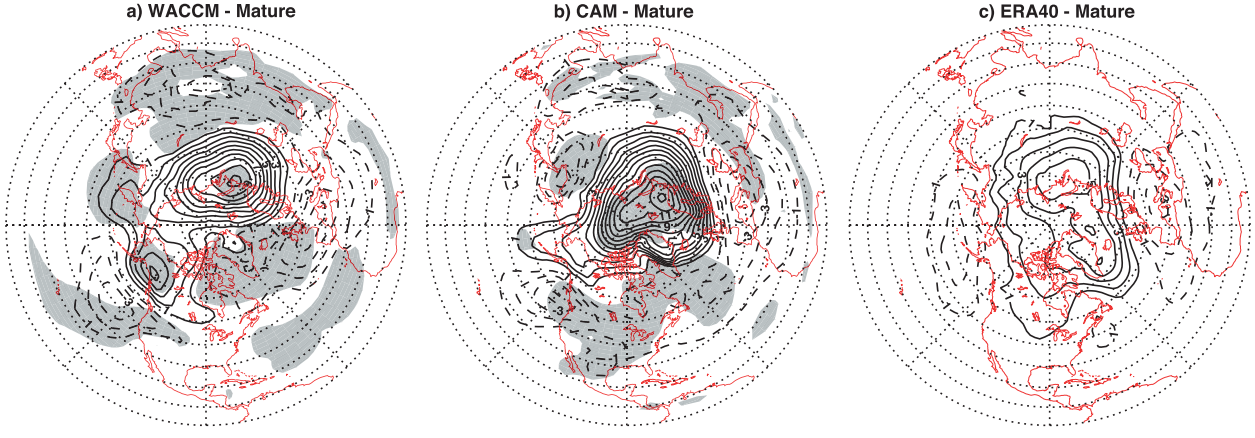

FIG. 7. Composite sea level pressure averaged between 7 days prior a stratospheric event and 7 days following the stratospheric weak events (mature stage) for (a) WACCM, (b) CAM, and (c) ERA-40. See text for the details of the calculation of the composites. Contour interval is 1 hPa; no zero contour is plotted. Shading in (a) and (b) indicates the 95% level of statistical confidence for each panel compared to (c).

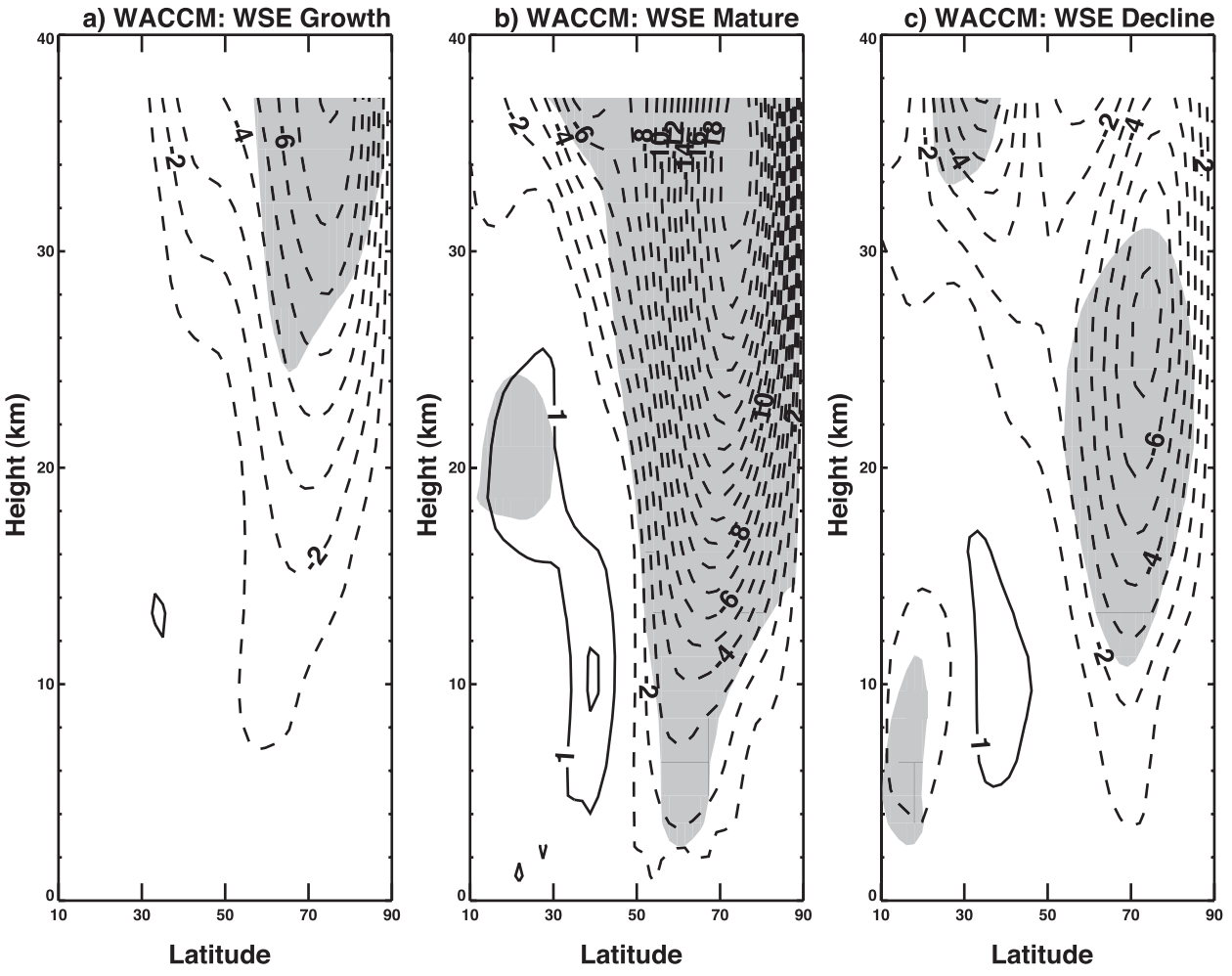

FIG. 8. Zonal mean zonal wind of WACCM composite life cycle of WSE during (a) growth (22–8 days prior the events), (b) maturity (7 days prior–7 days after the events), and (c) decline (8–22 days following the events) stages. Contour interval is 1 m s^{-1}. No zero contours are plotted. Shading indicates the 95% confidence interval based on a Student's *t*-test.

inside the polar vortex by several hundred meters in the midstratosphere. In the declining stage (Fig. 8c), the easterly wind anomaly is substantially reduced in the midstratosphere but the peak of the anomaly has descended further, to between 20 and 30 km. This is not only very similar to the real atmosphere (Fig. 10) but also reminiscent of the behavior seen in the January 2009 warming (Fig. 1).

The composite anomaly in CAM is illustrated in Fig. 9. As in WACCM, the temporal progression shows a strengthening of the zonal wind anomaly in the early stages of the WSE, followed by a weakening of the anomaly at later times. The magnitude of the anomalies is, however, much larger. Moreover, the easterly wind anomaly in the troposphere of CAM is at least twice as large as the corresponding anomaly in the analysis during the mature (Fig. 10b) and the declining stages (Fig. 10c), and the position of the peak anomaly in the stratosphere does not descend in CAM during the life cycle of the WSE but is always located near the model top.

It is important to note that the zonal wind anomalies at the mature stage of the stratospheric events (Figs. 8b–10b) are qualitatively consistent with the SLP pressure anomalies (Figs. 7a–c) at the same stage: as the zonal circulation of the polar vortex is decelerated during a WSE, the poleward mean meridional circulation strengthens and mass accumulates over the polar cap, resulting in a positive pressure anomaly at the surface. Notably, the SLP anomaly in the real atmosphere is weaker than in either model configuration. This is consistent with the zonal wind anomalies during the mature stage of the stratospheric event: at 12 km and 60°N, the zonal wind anomalies (Figs. 8b–10b) are respectively −5, −7, and −4 m s^{-1} in WACCM, CAM, and the analysis. As the zonal mean wind and temperature at high latitudes are in approximate geostrophic equilibrium, a stronger zonal wind negative

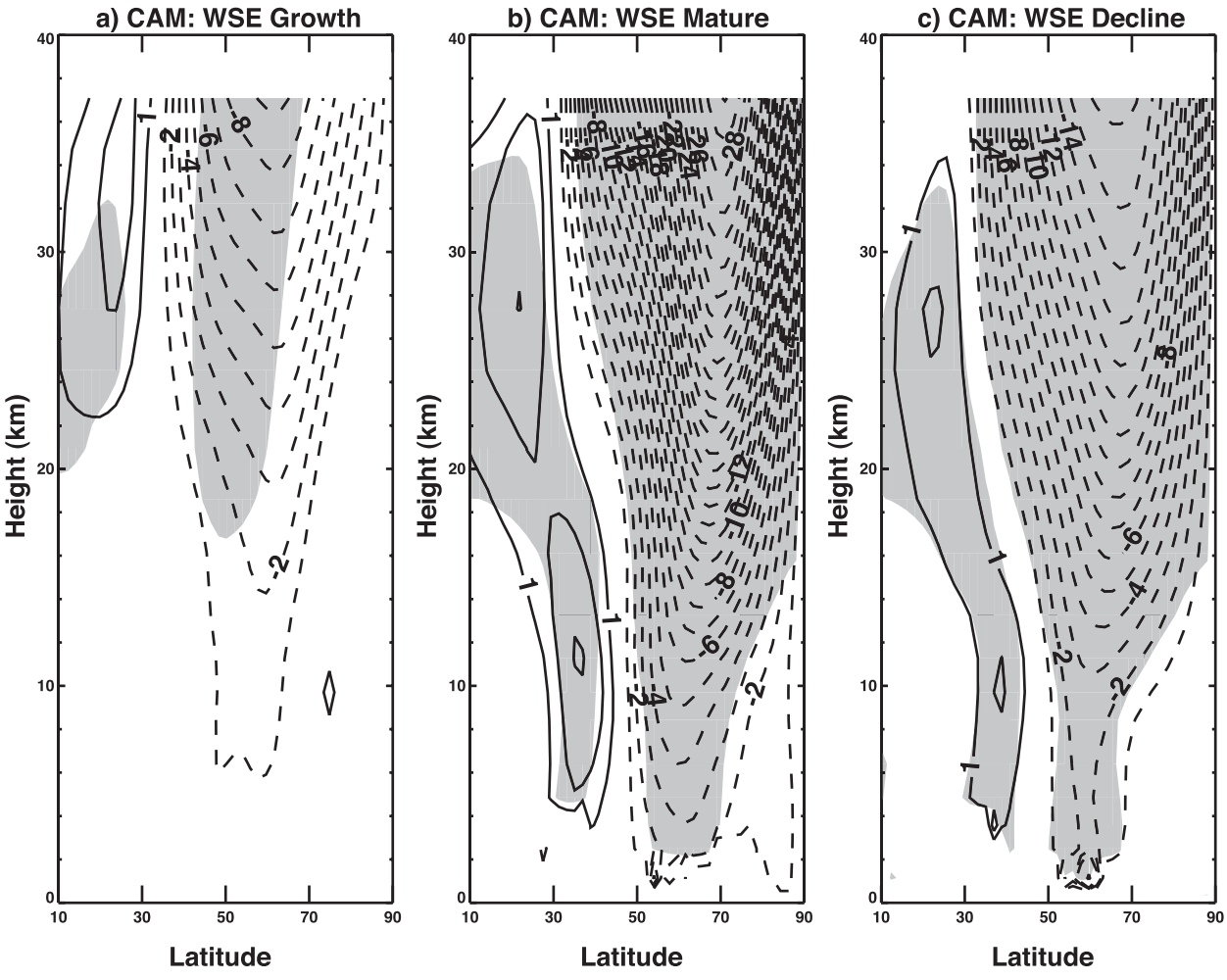

FIG. 9. As in Fig. 8, but for CAM.

anomaly in the lower stratosphere is accompanied by a warmer polar cap. This anomaly can be maintained against radiative dissipation only in the presence of a wave-driven poleward mean meridional circulation, which brings more mass into the polar cap.

From Figs. 8–10 it is possible to conclude qualitatively that poleward mass transport in the lower stratosphere and upper troposphere is stronger in CAM than in WACCM and stronger in either model than in the ERA-40 data. The detailed mass distribution that results from the poleward flow depends on the altitude and vertical structure of the mean meridional velocity field, but ultimately it is reflected in the zonal wind anomaly, which is in geostrophic balance with the mass field. This intuitive argument can be quantified if one takes the zonal anomalies in Figs. 8b–10b and calculates the mass perturbations implied by geostrophic and hydrostatic balance, as shown in the appendix.

Figure 11 shows the cumulative mass anomaly per unit area in a column over the polar cap (poleward of 60°N) for WACCM (solid black), CAM (dashed black), and the analysis (red) calculated from Eqs. (A6) and (A7) of the appendix. In all cases the mass increase is largest in the troposphere and lower stratosphere as a result of the density weighting of the integral (A6). The mass change, however, is much larger in CAM below 5 km than it is in WACCM or ERA-40. In particular, CAM produces a very large mass increase below 5 km that far exceeds what is seen in WACCM or in ERA-40. The mass perturbation in CAM is consistent with the larger zonal wind anomalies that penetrate deep into the troposphere in that model (cf. Figs. 8–10). The large increase in the CAM mass anomaly below 5 km is related to a zonal wind anomaly in the polar lower troposphere (Fig. 9, middle panel) that is not present in WACCM or ERA-40. In general, WACCM is much closer to the analysis than CAM, except that the mass change throughout the troposphere and lower stratosphere is somewhat larger at all levels than in the observations. Once again, this is consistent with the larger modification

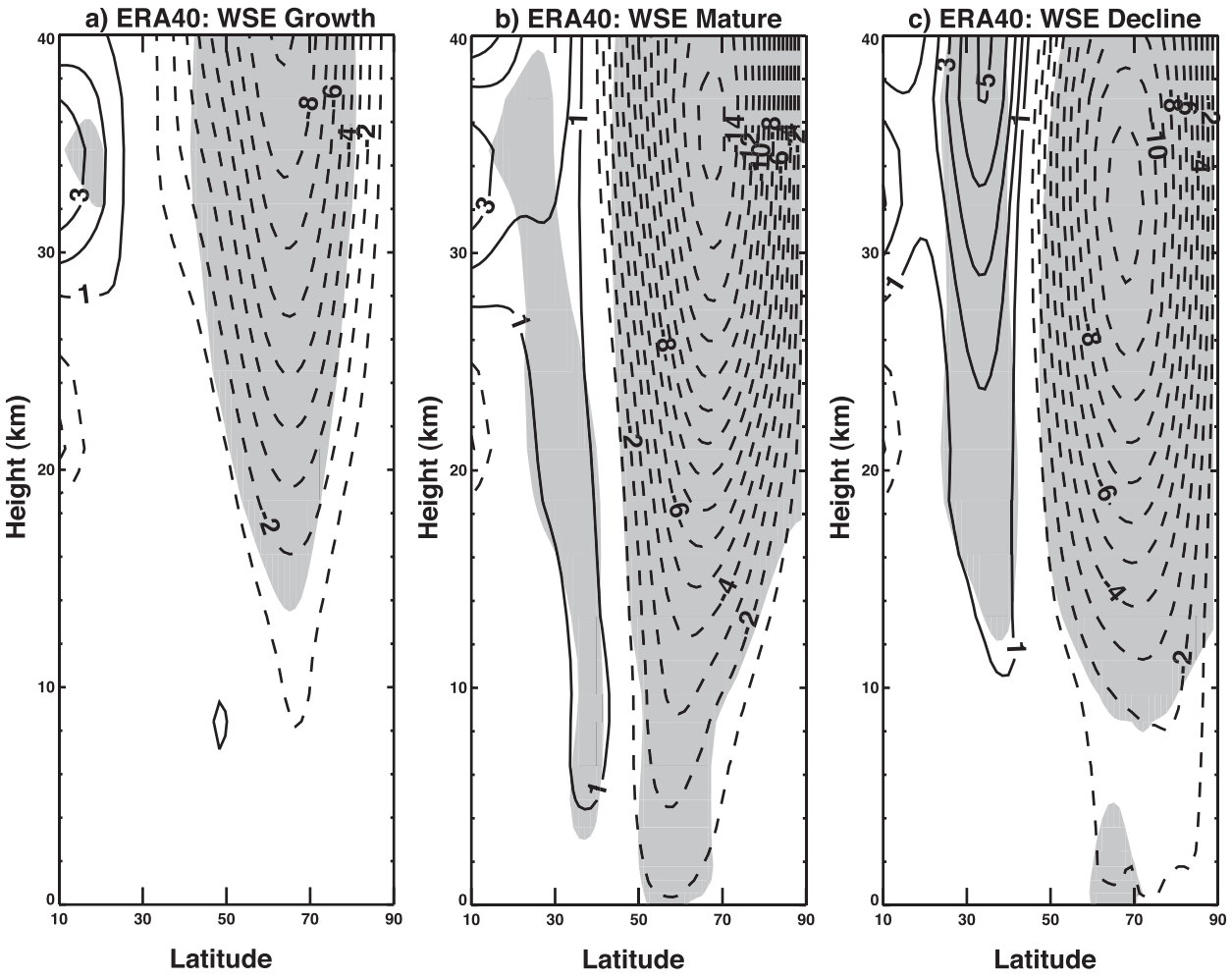

FIG. 10. As in Fig. 8, but for ERA-40.

of the zonal mean state that occurs in the model compared to the real atmosphere.

Figures 8–11 illustrate another interesting difference between the zonally averaged responses of the two model configurations: while the anomalies amplify realistically as the stratospheric events proceed from growth to mature stages, the anomaly maxima in CAM do not migrate downward with time but remain fixed near the model lid. This response in the low-lid model is unrealistic (cf. Baldwin and Dunkerton 2001).

The implications of these zonal wind anomalies for the surface behavior are summarized in Fig. 12, which shows the evolution of SLP anomalies averaged poleward of 60°N for WACCM (solid black), CAM (dashed black), and the analysis (solid red) between 90 days prior and 90 days following the WSE. In all cases the polar cap SLP increases during WSEs. However, the SLP increase in CAM is too large (~6 hPa) by about a factor of 2 compared to ERA-40. As discussed above, this is consistent with a polar vortex anomaly that is also too large and penetrates deep into the troposphere (Fig. 10b). On the other hand, the WACCM and ERA-40 SLP anomalies are closer in magnitude, although the maximum WACCM anomaly (−3.5 hPa) is still larger than ERA-40's (~3 hPa). The anomalies in WACCM and the analysis differ, moreover, in the evolution following the event: while the data show a gradual decrease as time proceeds, WACCM shows a more rapid decrease of polar SLP. These SLP anomalies are proportional to the mass perturbations shown in Fig. 11, since the SLP anomaly is just the mass anomaly times the acceleration of gravity (and divided by 100, if SLP is expressed in hPa). It should be noted that the 90% confidence interval for the results of Fig. 12 (evaluated using a Student's t test) is about 1.8 hPa: this interval is large enough that the anomalies are statistically distinguishable only around the mature stage when the differences are the largest. It follows that the ERA-40 and WACCM SLP are statistically

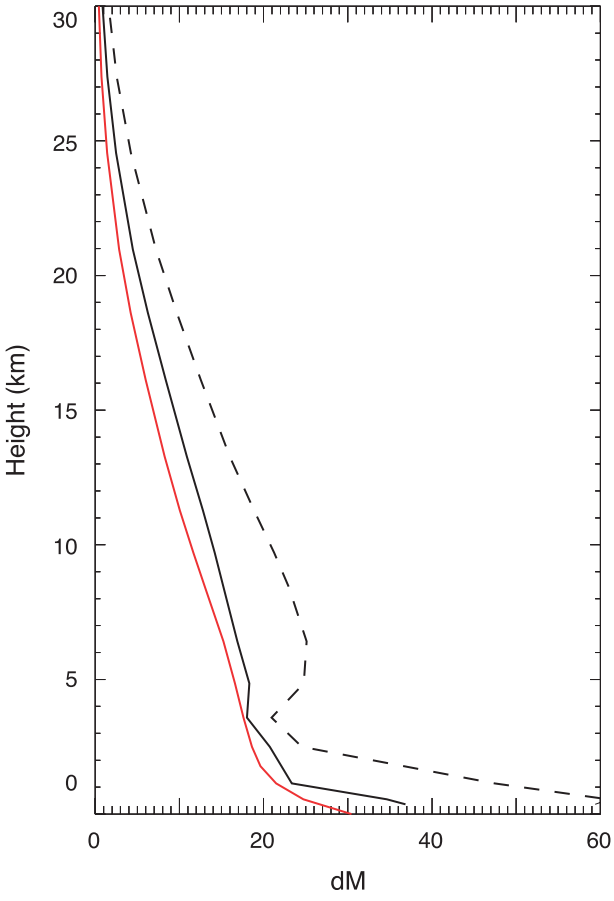

FIG. 11. Cumulative mass anomaly per unit area (kg m^{-2}) averaged over the NH polar cap (poleward of 60°N) obtained from the composite zonal wind at the mature stage of the weak stratospheric event (see the appendix). Solid black is WACCM, dashed black is CAM, and red is ERA-40.

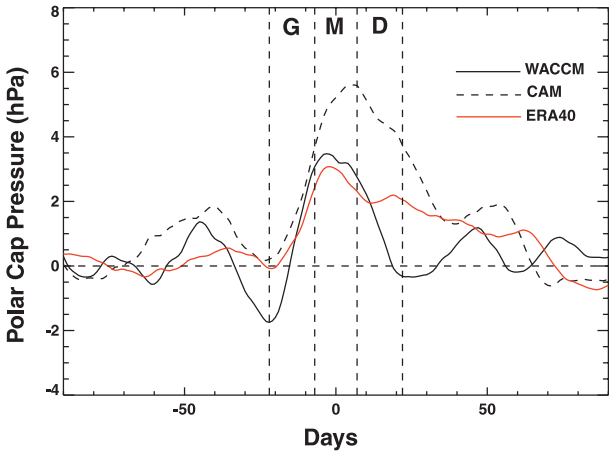

FIG. 12. Polar cap average of the sea level pressure from 90 days prior to 90 days following a WSE in WACCM (sold black), CAM (dashed black), and ERA-40 (red). The letters on top and the vertical dashed lines identify the growth (G), mature (M), and declining (D) stages as defined in the text.

indistinguishable during the mature stage, but SLP in CAM is statistically separated from both the high-top model and the reanalysis. It should be noted that the models predict an unrealistically large SLP increase from about day −21 to day 0; a similar pressure swing is not observed in the analysis products. Next we examine in greater detail this part of the composite cycle.

In Fig. 13 we show the polar projection of SLP anomalies for the models (Figs. 13a,b) and the reanalysis (Fig. 13c) during the growth stage (22–8 days prior to the WSE). This stage is worth inspecting because it illustrates the tropospheric behavior preceding the WSEs in the models and in the reanalysis. Both models, aside from some differences in the detailed structures, show a depression of the Arctic cap (more pronounced in WACCM) and a prominent wave-2 pattern poleward of 60°N. This horizontal structure is different from the composite behavior obtained from the ERA-40 reanalysis (Fig. 13c), which does not show a pronounced pressure decrease over the Arctic and displays a wave pattern at middle and high latitudes that is dominated by wave 1. Specifically in terms of the magnitude of the Arctic SLP depression, the model SLP is more akin to the behavior of the atmosphere during the largest SSWs. This is shown in Figs. 13d–f using the NAVDAS analysis during three recent SSWs: the large event of 21 January 2006 (Fig. 13d), the relatively small 22 February 2008 event (Fig. 13e), and again the large event of 24 January 2009 (Fig. 13f). For reference, the daily zonal mean zonal wind for each of these winters is shown in Figs. 13g–i. In the 2009 event the SLP (Fig. 13f) shows a complex horizontal structure with prominent wave-2 and wave-3 features, along with a substantial depression over the polar cap, as in the models. Similar behavior is obtained during the large SSW of 2006 (Fig. 13d). On the other hand, during the modest SSW of 2008, the SLP (Fig. 13e) does not show an Arctic depression. Based on the limited evidence provided by three cases, Fig. 13 suggests that the WSEs produced by the models are associated with tropospheric anomalies that are too large compared to the analysis data: only during the largest SSWs on record does the atmosphere present similar structures. This is apparently due to the fact that although the number of stratospheric events is smaller in the models than in the real atmosphere, the events that do occur are more intense and tend to distort the stratospheric vortex more than in reality.

5. Conclusions

Using two state-of-the-art climate models—1) a low-top model specifically designed to study the lower atmosphere (CAM) but with a poorly resolved middle atmosphere

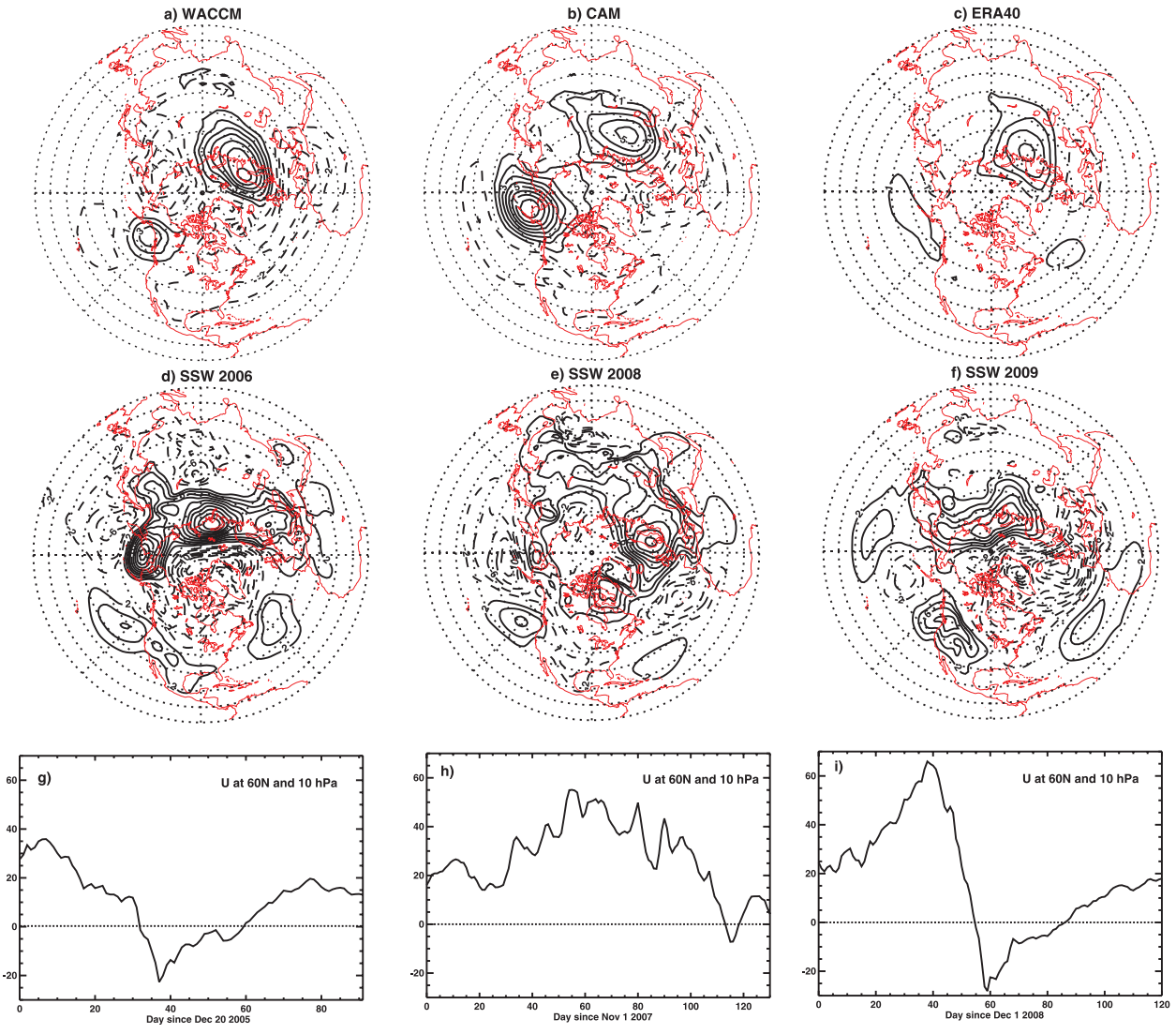

FIG. 13. (top) SLP during the growth stage of the WSE for (a) WACCM, (b) CAM, and (c) the ERA-40 reanalysis. (middle) SLP from the NAVDAS analysis during the growth stage of three SSWs: (d) 2006, (e) 2008, and (f) 2009. (bottom) Daily zonal mean zonal wind at 60°N and 10 hPa for each of the winters in (d)–(f). Contour intervals are (a)–(c) 1 hPa and (d)–(f) 2 hPa. No zero contours are plotted.

and 2) a high-top configuration that exploits the same physics of CAM in the lower atmosphere but is built to simulate realistically chemical and physical processes in the middle atmosphere (WACCM)—we have compared two present-day simulations coupled to a slab ocean model. The purpose of these simulations is to investigate how the winter climatology of the two model configurations is affected by the presence of a well-represented (numerically and physically) middle atmosphere. The main conclusions can be summarized as follows:

- Upper air and surface behavior are different between the two model configurations. While the time-mean differences were already pointed out in an earlier study (Boville and Cheng 1988), those differences are more pronounced during stratospheric anomalous vortex events and, in particular, weak vortex events. It should be borne in mind that the differences illustrated here are similar to but quantitatively different from Boville and Cheng (1988), in part because the stratosphere in the earlier study did not include important physical parameterizations, prominently a nonorographic mesoscale gravity wave parameterization.
- The differences of the zonal circulation originate directly from wave reflection from the upper lid in CAM. Zonal mean wind differences are largest near the model lid at 40 km but remain substantial and statistically significant even in the troposphere.

- During weak stratospheric events the two model configurations have qualitatively similar behavior but differ in the magnitude, persistence, and vertical progression of the perturbations. We have shown that the weak stratospheric events in CAM have larger amplitude than the corresponding events in WACCM.
- Wave reflection changes the stationary planetary wave structure in the stratosphere. Following on the conclusions of Boville and Cheng (1988), this process results directly in changes of the zonal mean state. On the other hand, we can conclude with relative confidence that there is no evidence of a direct influence of the upper model lid on the structure of tropospheric planetary waves. However, changes to the tropospheric behavior follow indirectly from the changes of the zonal mean circulation in the lower stratosphere/upper troposphere in the two model configurations during stratospheric weak events.
- The latitudinal mass redistribution during weak vortex events is reflected in the zonal mean zonal wind anomalies, since the zonal wind is in geostrophic balance with the temperature anomalies. Consistent with the larger magnitude and deeper penetration into the troposphere of negative zonal wind anomalies associated with weak stratospheric events, the mass changes are larger in the troposphere in the low-top model. This results in larger anomalies of SLP at the surface in CAM than in WACCM or the ERA-40 analysis. The mass redistribution and the SLP anomalies in WACCM, although still somewhat larger than in the analysis, are closer to observations.
- Inspection of the sea level pressure shows that the model simulations of weak stratospheric events are characterized by a large and prominent wave-2 pattern. Compared to the climatological behavior in ERA-40 data, this surface pattern is too vigorous. On the other hand, it is more akin to observed behavior during very large weak stratospheric events and persistent stratospheric wind reversals.

The main conclusion of this study is that a poorly resolved stratosphere affects the atmospheric behavior both in the stratosphere and in the troposphere, including the surface pressure field. We have illustrated how the stratospheric variability and in particular the state of a weak stratospheric polar night jet influences the troposphere. Our results show clearly that more realistic simulations are obtained in a model that includes the middle atmosphere. The importance of these effects in the context of a changing climate is an open question.

Acknowledgments. The authors thank J. Perlwitz for comments on this manuscript. Comments from three anonymous reviewers are greatly appreciated. FS was supported by the Office of Naval Research through NRL's base 6.1 research program.

APPENDIX

Relationship among Zonally Averaged Mass, Temperature, and Zonal Wind Anomalies under Geostrophic and Hydrostatic Equilibrium

Consider the hydrostatic equation in geometric coordinates z_g:

$$\frac{\partial p}{\partial z_g} = -\rho g, \tag{A1}$$

where p is the pressure, ρ is the air density, and g is the acceleration of gravity. Equation (A1) can be rewritten as

$$dp = -g dM, \tag{A2}$$

where dM is the mass element per unit area. Transforming Eq. (A2) into log-pressure vertical coordinates, $z = H \ln(p_0/p)$ yields

$$\frac{p}{H}\, dz = g dM, \tag{A3}$$

where H is the atmospheric scale height.

Rearranging Eq. (A3) gives the mass element in log-pressure coordinates:

$$dM = \frac{p}{gH}\, dz, \tag{A4}$$

and substituting $H = RT_0/g$ and $p = \rho RT$, where R is the gas constant and T_0 is the reference temperature, yields

$$dM = \rho_0 \frac{T(z)}{T_0} \exp(-z/H)\, dz, \tag{A5}$$

where we have also used the fact that $\rho = \rho_0 \exp(-z/H)$ in log-pressure coordinates, with ρ_0 being the air density at the surface.

Integrating Eq. (A5) from the top of the atmosphere to an arbitrary level z we obtain the cumulative mass anomaly at z:

$$M(z) = \frac{\rho_0}{T_0} \int_{\infty}^{z} T(z) \exp(-z/H)\, dz. \tag{A6}$$

The mass anomaly given by Eq. (A6) is related to the zonal wind anomaly by hydrostatic and geostrophic balance:

$$T = \frac{H}{R}\frac{\partial \phi}{\partial z} \quad \text{and} \quad u = -\frac{1}{f}\frac{\partial \phi}{a\partial \theta}, \tag{A7}$$

where ϕ is the geopotential, f is the Coriolis parameter, a is the earth's radius, and θ is the latitude. Therefore, from a given zonal wind anomaly in hydrostatic and geostrophic equilibrium it is possible to determine the mass perturbations in the column from Eq. (A6).

In practice, the calculation proceeds as follows: from the zonal wind anomalies, the geopotential is calculated from geostrophic balance [the second term in Eq. (A7)]; the geopotential is constrained to conserve mass by subtracting the horizontal average at each level; the resulting geopotential is used to calculate the temperature anomalies using hydrostatic balance [the first term in Eq. (A7)]; and finally the mass anomaly is calculated from Eq. (A6).

REFERENCES

Baldwin, M. P., and T. J. Dunkerton, 1999: Propagation of the Arctic Oscillation from the stratosphere to the troposphere. *J. Geophys. Res.,* **104,** 30 937–30 946.

——, and ——, 2001: Stratospheric harbingers of anomalous weather regimes. *Science,* **294,** 581–584.

Boville, B. A., 1984: The influence of the polar night jet on the tropospheric circulation in a GCM. *J. Atmos. Sci.,* **41,** 1132–1142.

——, and X. Cheng, 1988: Upper boundary effects in a general circulation model. *J. Atmos. Sci.,* **45,** 2591–2606.

Charlton, A. J., and Coauthors, 2007: A new look at stratospheric sudden warmings. Part II: Evaluation of numerical model simulations. *J. Climate,* **20,** 470–488.

Charney, J. G., and P. G. Drazin, 1961: Propagation of planetary-scale disturbances from the lower into the upper atmosphere. *J. Geophys. Res.,* **66,** 83–109.

Collins, W. D., and Coauthors, 2004: Description of the NCAR Community Atmosphere Model (CAM3.0). NCAR Tech. Note NCAR/TN-464+STR, 214 pp.

——, and Coauthors, 2006: The formulation and atmospheric simulation of the Community Atmosphere Model version 3 (CAM3). *J. Climate,* **19,** 2144–2161.

Eckermann, S. D., and Coauthors, 2009: High-altitude data assimilation system experiments for the northern summer mesosphere season of 2007. *J. Atmos. Solar-Terr. Phys.,* **71,** 531–551.

Eyring, V., and Coauthors, 2005: A strategy for process-oriented validation of coupled chemistry–climate models. *Bull. Amer. Meteor. Soc.,* **86,** 1117–1133.

——, and Coauthors, 2007: Multi-model projections of stratospheric ozone in the 21st century. *J. Geophys. Res.,* **112,** D16303, doi:10.1029/2006JD008332.

Garcia, R. R., D. R. Marsh, D. E. Kinnison, B. A. Boville, and F. Sassi, 2007: Simulation of secular trends in the middle atmosphere, 1950–2003. *J. Geophys. Res.,* **112,** D09301, doi:10.1029/2006JD007485.

Hoppel, K. W., N. L. Baker, L. Coy, S. D. Eckermann, J. P. McCormack, G. Nedoluha, and D. E. Siskind, 2008: Assimilation of stratospheric and mesospheric temperatures from MLS and SABER into a global NWP model. *Atmos. Chem. Phys.,* **8,** 6103–6116.

Kinnison, D. E., and Coauthors, 2007: Sensitivity of chemical tracers to meteorological parameters in the MOZART-3 chemical transport model. *J. Geophys. Res.,* D20302, doi:10.1029/2006JD007879.

Kodera, K., Y. Kuroda, and S. Pawson, 2000: Stratospheric sudden warmings and slowly propagating zonal mean zonal wind anomalies. *J. Geophys. Res.,* **105,** 12 351–12 359.

Limpasuvan, V., D. W. J. Thompson, and D. L. Hartmann, 2004: The life cycle of the Northern Hemisphere sudden stratospheric warmings. *J. Climate,* **17,** 2584–2596.

Lin, S.-J., 2004: A ''vertically-Lagrangian'' finite-volume dynamical core for global atmospheric models. *Mon. Wea. Rev.,* **132,** 2293–2307.

Liu, H.-L., F. Sassi, and R. R. Garcia, 2009: Error growth in a whole atmosphere climate model. *J. Atmos. Sci.,* **66,** 173–186.

Manney, G. L., and Coauthors, 2009: Aura Microwave Limb Sounder observations of dynamics and transport during the record-breaking Arctic stratospheric major warming. *Geophys. Res. Lett.,* **36,** L12815, doi:10.1029/2009GL038586.

Manzini, E., M. A. Giorgetta, M. Esch, L. Kornblueh, and E. Roeckner, 2006: The influence of sea surface temperatures on the northern winter stratosphere: Ensemble simulations with the MAECHAM5 model. *J. Climate,* **19,** 3863–3881.

McFarlane, N. A., 1987: The effect of orographically excited gravity wave drag on the general circulation of the lower stratosphere and troposphere. *J. Atmos. Sci.,* **44,** 1775–1800.

Perlwitz, J., and N. Harnik, 2004: Downward coupling between the stratosphere and troposphere: The relative roles of wave and zonal mean processes. *J. Climate,* **17,** 4902–4909.

Polvani, L. M., and D. W. Waugh, 2004: Upward wave activity flux as precursor to extreme stratospheric events and subsequent anomalous surface weather regimes. *J. Climate,* **17,** 3548–3554.

Richter, J. H., F. Sassi, K. Matthes, R. R. Garcia, and C. A. Fischer, 2008: Dynamics of the middle atmosphere as simulated by the Whole Atmosphere Community Climate Model, version 3 (WACCM3). *J. Geophys. Res.,* **113,** D08101, doi:10.1029/2007JD009269.

——, ——, and R. R. Garcia, 2010: Toward a physically based gravity wave source parameterization in a general circulation model. *J. Atmos. Sci.,* **67,** 136–156.

Rind, D., J. Perlwitz, and P. Lonergan, 2005: AO/NAO response to climate change: 1. Respective influences of stratospheric and tropospheric climate changes. *J. Geophys. Res.,* **110,** D12107, doi:10.1029/2004JD005103.

Sassi, F., D. Kinnison, B. A. Boville, R. R. Garcia, and R. Roble, 2004: Effect of El Niño–Southern Oscillation on the dynamical, thermal, and chemical structure of the middle atmosphere. *J. Geophys. Res.,* **109,** D17108, doi:10.1029/2003JD004434.

——, B. A. Boville, D. Kinnison, and R. R. Garcia, 2005: The effects of interactive ozone chemistry on simulations of the middle atmosphere. *Geophys. Res. Lett.,* **32,** L07811, doi:10.1029/2004GL022131.

Shaw, T. A., and T. G. Shepherd, 2007: Angular momentum conservation and gravity wave drag parameterization: Implications for climate models. *J. Atmos. Sci.,* **64,** 190–203.

Solomon, S., D. Qin, M. Manning, M. Marquis, K. Averyt, M. M. B. Tignor, H. L. Miller Jr., and Z. Chen, Eds., 2007: *Climate Change 2007: The Physical Science Basis*. Cambridge University Press, 996 pp.

Yukimoto, S., and K. Kodera, 2007: Annular modes forced from the stratosphere and interactions with the oceans. *J. Meteor. Soc. Japan,* **85,** 943–952.